

# Outflowing material in the CSS quasar 3C48: evidence of jet-cloud interaction?

Neeraj Gupta<sup>1\*</sup>, R. Srianand<sup>2</sup> and D.J. Saikia<sup>1</sup>

<sup>1</sup>National Centre for Radio Astrophysics, TIFR, Pune 411 007, India

<sup>2</sup>Inter-University Centre for Astronomy and Astrophysics, Pune 411 007, India

Accepted. Received; in original form

## ABSTRACT

We report the detection of a  $z_{\text{abs}}=0.3654$  associated absorption-line system in the UV spectrum of the CSS quasar 3C48. The absorbing material is blue shifted with respect to the quasar emission-line redshift,  $z_{\text{em}}=0.3700$ , suggesting an outflow velocity of  $\sim 1000 \text{ km s}^{-1}$ . We detect absorption lines over a range of ionization states from Ly $\beta$ , Ly $\gamma$ , C IV, N IV, S VI to O VI and possibly O IV and Ne VIII. The kinematical properties of the absorption-line system are similar to the blue-shifted emission line gas seen in [OIII]  $\lambda 5007$  (Chatzichristou, Vanderriest & Jaffe 1999), which is believed to have interacted with the radio jet. We study the properties of the absorbing material using CLOUDY and find that photoionization models with Solar abundance ratios (with overall metallicity in the range  $0.1 \leq Z/Z_{\odot} \leq 1.3$ ) are enough to explain the observed column densities of all the species except Ne VIII, detection of which requires confirmation. Since the cooling and recombination time for the gas is  $\sim 10^5$  yr, the consistency with the photoionization models suggests that any possible interaction of absorbing material with the jet must have taken place before  $\sim 10^5$  yr. The abundance ratio of nitrogen to carbon is close to Solar values, unlike in the case of most quasars, especially at high-redshifts, which have super-Solar values. We observed 3C48 with the Giant Metrewave Radio Telescope (GMRT) to search for redshifted 21cm H I absorption. However, we did not detect any significant feature in our spectra and estimate the  $3\sigma$  upper limit to the optical depth to be in the range 0.001 to 0.003. However, due to the diffuse nature of the radio source, optical depths as high as 0.1 towards individual knots or compact components cannot be ruled out.

**Key words:** galaxies: active – galaxies: jets – quasars: absorption lines – quasars: individual: 3C48.

## 1 INTRODUCTION

Compact steep-spectrum sources (CSSs) are defined to be radio sources with projected linear size  $\lesssim 20 \text{ kpc}$  ( $H_0=71 \text{ km s}^{-1} \text{ Mpc}^{-1}$ ,  $\Omega_m=0.27$ ,  $\Omega_{\Lambda}=0.73$ , Spergel et al. 2003) and having a steep high-frequency radio spectrum ( $\alpha \gtrsim 0.5$ , where  $F(\nu) \propto \nu^{-\alpha}$ ). High-resolution radio images of CSSs show that there is a wide variety of structures, ranging from double-lobed and triple sources to those which are very complex and distorted (e.g. Phillips & Mutel 1982; Spencer et al. 1989; Fanti et al. 1990; Conway et al. 1994; Wilkinson et al. 1994; Sanghera et al. 1995; Dallacasa et al. 1995; Readhead et al. 1996a; Taylor et al. 1996; Snellen et al. 2000a; Stanghellini et al. 2001; Orienti et al. 2004). Although there is a consensus of opinion that most CSSs are young radio

sources (Fanti et al. 1995; Readhead et al. 1996b; O’Dea 1998 for a review; Snellen et al. 2000b), a small fraction could be confined to small dimensions due to either a dense medium or interactions of the jet with dense clouds. Radio studies have shown that CSSs tend to be more asymmetric than the larger sources, possibly due to interaction with an asymmetric distribution of gas in the central regions (Saikia et al. 1995, 2001; Saikia & Gupta 2003). These authors speculated that this might be due to collisions with clouds of gas, some of which fuel the nuclear activity. Arshakian & Longair (2000) also concluded that intrinsic/environmental asymmetries are more important for sources of small physical sizes. Radio polarization studies often indicate large Faraday depths (e.g. Mantovani et al. 1994; Fanti et al. 2004), and also sometimes show evidence of asymmetrically-located clouds as a huge differential rotation measure between the oppositely directed lobes as in the CSS quasar 3C147 (Junor et al. 1999), or high rotation measure where the jet bends

\* E-mail: neeraj@ncra.tifr.res.in (NG); anand@iucaa.ernet.in (RS); djs@ncra.tifr.res.in (DJS)

**Table 1.** Observational log of UV data

Program ID	Instrument used	PI	Exposure time (s)	Wavelength coverage (Å)	Resolving power (R)	Signal-to-noise (per spectral resolution)
9280	HST STIS	A. Siemiginowska	8,113	2049–2139	11,000	7
8299	HST STIS	W. Jaffe	5,280	8540–9107	8,500	20
6707	HST GHRS	D. Bowen	21,760	1287–1575	2,000	15–25
Z002	FUSE	P. Wannier	8,347	985–1084	20,000	7 <sup>a</sup>
KQ003	IUE	O’Brien	24,960	1150–1979	250	4

<sup>a</sup> The FUSE spectrum has been smoothed over 15 pixels.

sharply suggesting collision of the jet with a dense cloud as in 3C43 (Cotton et al. 2003). Optical studies of CSSs have also often shown evidence of interaction of the radio jets with the external medium (e.g. Gelderman & Whittle 1994; de Vries et al. 1999; Axon et al. 2000; O’Dea et al. 2002). The physical conditions under which a jet may be bent or distorted by such clouds, as well as the effects of an asymmetric gas distribution on opposite sides of the nucleus have been explored via analytical calculations as well as numerical simulations (Carvalho 1998; Higgins, O’Brien & Dunlop 1999; Wang, Wiita & Hooda 2000; Jeyakumar et al. 2005).

An interesting way of investigating the interaction of the jet with the external clouds/medium could be via the absorption lines arising from the clouds accelerated by the jet. Baker et al. (2002) have studied the absorption spectra in a sample of quasars selected from the Molonglo Reference Catalogue, and find a slight excess of blue-shifted C IV absorption lines in CSSs compared with the larger objects. In a sample of high-redshift radio galaxies, van Ojik et al. (1997) reported a high incidence of H I absorption (9 out of 10) in the smaller objects (<50 kpc) compared with the larger ones (2 out of 8). Their study also showed an excess of blue-shifted Ly $\alpha$  absorption lines, and showed strong evidence of interaction of the radio source with the external environment. Although blue-shifted absorption lines could arise due to either halo gas or circumnuclear gas kinematically affected by nuclear winds and/or radiation pressure, such studies suggest that jet-cloud interaction may also play a significant role in these objects.

To explore this theme, we have studied the well-known CSS quasar 3C48, which has a highly complex and distorted radio structure, speculated to be due to disruption of the jet by interaction with a cloud (e.g. Wilkinson et al. 1991; Worrall et al. 2004; Feng et al. 2005). We explore evidence of blue-shifted absorption line gas at radio and ultraviolet (UV) wavelengths using the Giant Metrewave Radio Telescope (GMRT) and archival, but previously unpublished, data from the Hubble Space Telescope (HST) Space Telescope Imaging Spectrograph (STIS) and the Goddard High Resolution Spectrograph (GHRS), the Far Ultraviolet Spectroscopic Explorer (FUSE) and the International Ultraviolet Explorer (IUE). We report the detection of blue-shifted absorption line gas, examine the physical properties of the absorber and discuss the possibility that this might be accelerated by interaction with the radio jet.

## 2 3C48

3C48, the second quasar to be identified (Mathews & Sandage 1963), is an enigmatic CSS source. It has unusually strong IR emission (Neugebauer, Soifer & Miley 1985), comparable with most luminous IR galaxies. The detection of CO emission (Scoville et al. 1993; Wink, Guilloteau & Wilson 1997) at  $z=0.3695$  implies the presence of about twice as much molecular gas as in ULIRGs. At radio wavelengths, the VLBI images resolve this highly compact radio source into a one-sided core-jet structure confined well within the optical host galaxy. Briggs (1995) and Feng et al. (2005) have reported the detection of a weak counter-jet on subarcsec scales. Wilkinson et al. (1991) interpret the complex structure of 3C48 as due to collision of the jet with a dense clump of gas in the host galaxy’s interstellar medium. The radio jet is also aligned with the excess optical continuum, and [OII]  $\lambda 3727$  and [OIII]  $\lambda\lambda 4959, 5007$  emission-line nebulosity seen close to the quasar core, and in particular the peak of continuum light at about 1 arcsec from the nucleus. This has been variously interpreted as the nucleus of a galaxy, merging with the host of 3C48 (Stockton & Ridgway 1991) or a star-forming region triggered by the radio jet (Chatzichristou et al. 1999).

The redshift of 3C48 as measured by several authors (Greenstein & Mathews 1963; Wampler et al. 1975; Thuan, Oke & Bergeron 1979) differ by about  $\sim 500 \text{ km s}^{-1}$ . In particular, Boroson & Oke (1982) noted that redshift of 3C48 as determined from the forbidden emission lines turns out to be slightly less than the value of  $0.3700 \pm 0.0002$  determined from the permitted emission lines. The discrepancy arose largely due to the lower spectral resolution data. In the higher resolution data of Chatzichristou et al. (1999), the forbidden lines are resolved into two components, one of which shows velocities similar to the permitted lines. The value of 0.3700 is also in agreement with the emission lines and stellar absorption lines seen from the fuzz around the source. The MgII emission line (Tytler et al. 1987) and CO emission (Scoville et al. 1993) have also been seen at redshifted frequencies corresponding to  $\sim 0.370$ . Therefore, throughout this paper we use  $z_{\text{em}} = 0.3700$  to represent the quasar redshift.

## 3 OBSERVATIONS AND DATA ANALYSES

We first describe the analyses of the archival but previously unpublished UV data from HST STIS and GHRS, FUSE and IUE. These data have been obtained from the Multimis-

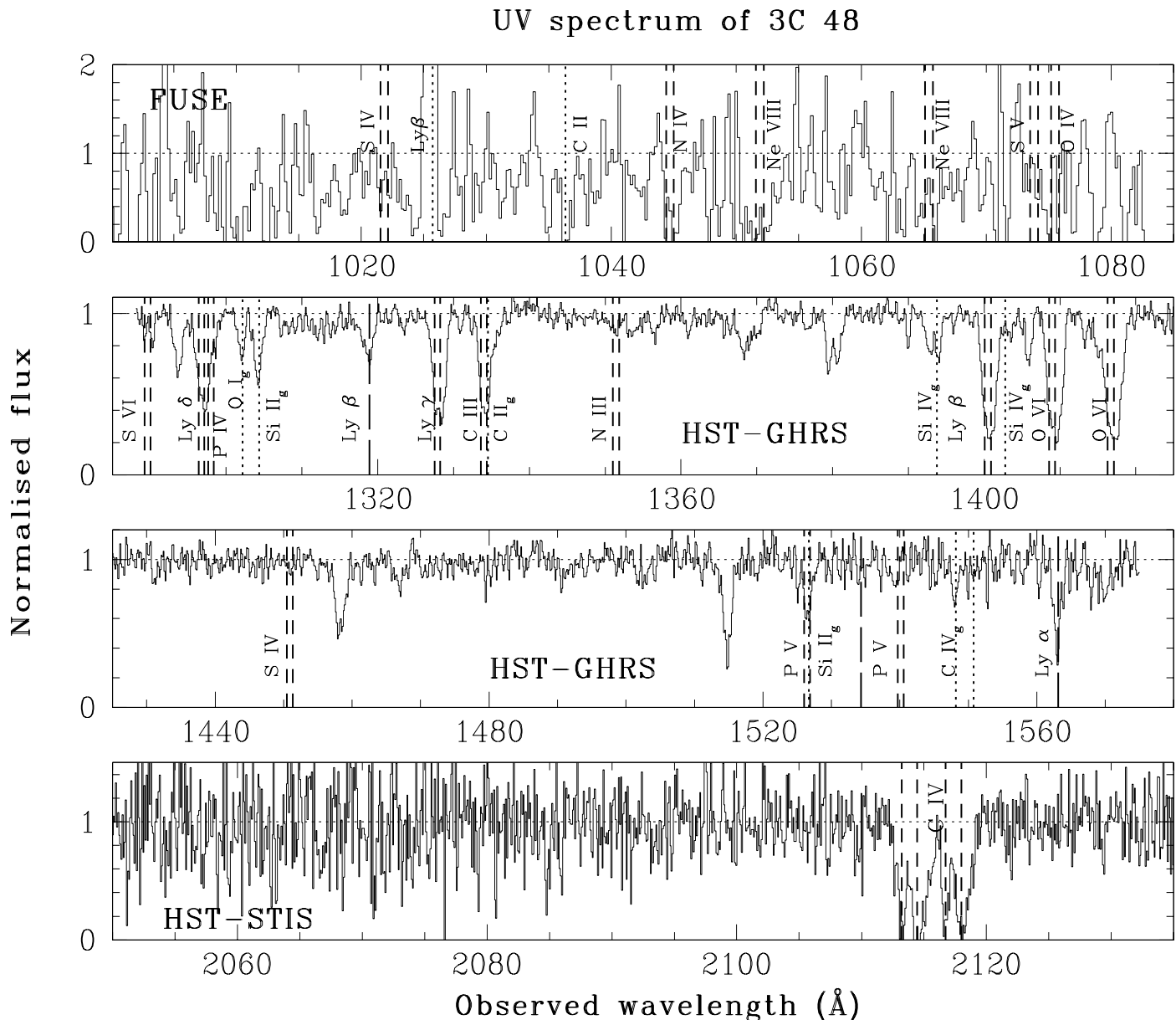


**Figure 1.** UV spectrum of the  $z_{em} = 0.3700$  quasar 3C48. Different absorption lines are labelled. Vertical dashed lines represent the positions of the absorption components associated with the  $z_{abs}=0.3649$  and  $0.3658$  systems. Short-dashed lines with the label ‘g’ correspond to Galactic absorption. Long dashed lines mark a possible intervening system,  $z_{abs}=0.286$ . A number of unidentified absorption features (left unmarked) are also present in the spectrum. It is most likely that these are intervening Ly $\alpha$  absorption lines.

sion Archive at Space Telescope (MAST). We then describe the radio observations with the GMRT to detect redshifted H I in absorption towards 3C48.

### 3.1 UV data

The data from HST STIS and GHRS, FUSE and IUE instruments were reduced using the standard pipeline tasks `calstis`, `calhrs`, `calfuse` and `caliue` respectively. The pipeline processing keeps track of errors associated with each pixel at every stage of the reduction. The spectra corresponding to various exposures for each instrument along with the error spectra were then combined separately. The

resulting signal-to-noise ratio applicable over most of the wavelength range and some of the basic details of the data sets used are summarised in Table 1. The spectra for each of the data sets were then continuum fitted using absorption free regions to get the final spectrum shown in Fig. 1.

The pipeline tasks also process the line lamp exposures to determine the zero point offset of wavelength and spatial scales in the image. We also made use of the Galactic absorption lines detected in each of the spectra to determine the zero point offsets. In particular, for the GHRS spectrum we find that it is required to shift the spectrum by approximately  $+0.8 \text{ \AA}$ . This is also consistent with the rms of approximately one diode (roughly  $0.6 \text{ \AA}$ ) in the de-

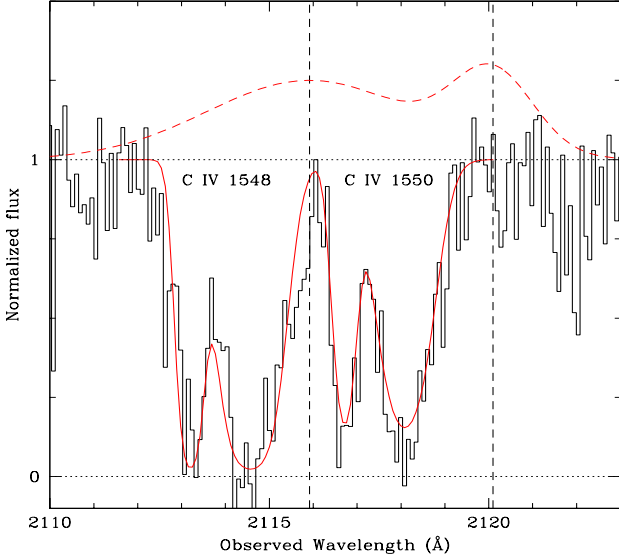


**Figure 2.** Profile of C IV  $\lambda\lambda 1548, 1550$  absorption lines detected in the STIS spectrum of 3C48 (histogram) overplotted with the best-fitted Voigt profiles (smooth curves). Two well-detached absorption components are detected clearly at  $z_{\text{abs}} = 0.3649$  and  $0.3658$ . Vertical long-dashed lines mark the expected location of C IV  $\lambda 1548$  emission based on the two velocity components detected in [O III]  $\lambda\lambda 4959, 5007$  and [O II]  $\lambda 3727$  emission lines (Chatzichristou et al. 1999). The figure also shows the expected velocity range of emitting gas (Gaussians with long-dashed lines) reconstructed using the parameters of Chatzichristou et al. (1999). The gas producing the C IV absorption is well detached from the nuclear line-emitting gas and has a velocity consistent with the blue component of the narrow line-emitting gas.

fault wavelength scale of GHRS pipeline calibration. The one diode rms in the wavelength scale arises due to the errors in the carousel positioning and uncertainties caused due to the changing temperatures within the spectrograph and geomagnetically induced image motions (see *Instrument Handbook for the GHRS* for details). The spectrum corresponding to three GHRS exposures were combined after applying this offset.

### 3.2 Radio observations with GMRT

We observed 3C48 with GMRT to investigate redshifted 21cm absorption with a bandwidth of 4 MHz in the 1060 MHz subband. The FX correlator system at GMRT splits the baseband bandwidth into 128 spectral channels, yielding a spectral resolution of  $8.75 \text{ km s}^{-1}$  for the chosen bandwidth. We observed 3C48 on a number of occasions with the redshifted 21cm frequencies corresponding to  $z_{\text{abs}} = 0.3654$ , the redshift at which we detect outflowing gas (Section 4) and  $0.3695$  and  $0.3700$ , the emission-line redshifts from CO and optical observations respectively. This object was observed as part of a larger survey of H I absorption towards CSSs, and the observational details will be described in more detail elsewhere. The radio data were reduced in the standard way using the Astronomical Image Processing System.

## 4 OBSERVATIONAL RESULTS

### 4.1 UV spectra

We detect blue-shifted absorption lines with  $z_{\text{abs}} \simeq z_{\text{em}}$  in the UV spectra of 3C48. Fig. 1 shows the normalised UV spectrum obtained with HST and FUSE. Expected positions of absorption lines from our Galaxy, the associated system at  $z_{\text{abs}} = 0.3654$  and an intervening Ly $\alpha$  system at  $z_{\text{abs}} = 0.286$  are marked with short-dashed, dashed and long-dashed vertical lines respectively. In the case of the  $z_{\text{abs}} = 0.3654$  system we have marked the locations of the two velocity components identified from the C IV  $\lambda\lambda 1548, 1550$  absorption lines seen in the STIS spectrum. It is clear from the figure that Ly $\beta$ , Ly $\gamma$ , Ly $\delta$ , C IV, O VI and S VI absorption lines from the  $z_{\text{abs}} = 0.3654$  system are present in the HST-STIS and GHRS spectra. The C III  $\lambda 977$  absorption line is possibly blended with C II  $\lambda 1334$  absorption from our Galaxy. We find Ly $\delta$  to be slightly stronger than the Ly $\gamma$  line, which is possibly because of blending with the P IV absorption line.

Absorption lines of P V doublets and S IV are clearly absent. The available spectra do not cover the wavelength range where Ly $\alpha$ , N V and Si IV absorption lines are expected. The FUSE spectrum is noisier and we have examined the different exposures independently to verify the reliability of absorption lines. We have detected N IV and possibly O IV and Ne VIII. To our knowledge, Ne VIII absorption has been reported for 5 other systems, namely 3C288.1, UM 675, HS 1700+6416, J2233–606 and SBS 1542+531 (Petitjean, Riediger & Rauch 1996; Petitjean & Srianand 1999; Hamann et al. 1997; Telfer et al. 1998; Hamann, Netzer & Shields 2000). Based on the presence of absorption due to very highly ionized species and  $z_{\text{abs}} \simeq z_{\text{em}}$  it is most likely that the gas responsible for the absorption is located close to the nuclear region of 3C48.

The C IV  $\lambda\lambda 1548, 1550$  absorption doublet detected in the STIS data is clearly resolved into two components at  $z_{\text{abs}} = 0.3649$  and  $0.3658$  (Fig. 2). Voigt profile decomposition gives,  $N(\text{C IV}) = 3.44 \pm 0.55 \times 10^{14} \text{ cm}^{-2}$ ,  $b = 39.8 \pm 4.3 \text{ km s}^{-1}$  and  $N(\text{C IV}) = 7.91 \pm 0.74 \times 10^{14} \text{ cm}^{-2}$ ,  $b = 92.6 \pm 5.9 \text{ km s}^{-1}$  respectively for these components. Within the errors of the STIS spectrum, it cannot be ruled out that the C IV  $\lambda\lambda 1548, 1550$  absorption lines are not saturated. Therefore, we take the column density estimates from the Voigt profile fits as a lower limit. In Fig. 2, along with the Voigt-profile fits to C IV absorption line, we show the location of C IV  $\lambda 1548$  emission as expected from the two components detected in the [O III]  $\lambda\lambda 4959, 5007$  and [O II]  $\lambda 3727$  emission lines (Chatzichristou et al. 1999). From the two-component profile decomposition of the emission-line spectrum integrated over the central  $1.9 \text{ arcsec}^2$ , Chatzichristou et al. (1999) find that one of the components (referred to as the red component) have redshift similar to the systemic redshift of the quasar while the other component (referred to as the blue component) is blue shifted by  $\sim 580 \pm 15 \text{ km s}^{-1}$ . The systemic red component is much narrower (FWHM  $\sim 400 \text{ km s}^{-1}$ ) and shows a systematic trend in the velocity structure suggesting association with the rotational velocity field of the galaxy. The blue component on the other hand has much wider (FWHM  $\sim 1010 \text{ km s}^{-1}$ ) line profile and shows no clear trend in the velocity field structure. From Fig. 2 it is clear that (i) the absorbing gas completely covers the background source and (ii) the velocity range spanned

by the absorbing gas is consistent with that of the outflowing gas responsible for the blue-shifted [OIII]  $\lambda\lambda 4959, 5007$  and [OII]  $\lambda 3727$  emission detected by Chatzichristou et al. (1999).

In the lower-resolution GHRS data, the two absorption components detected in the STIS spectrum are unresolved. However the widths of the detected absorption lines are consistent with the presence of two components that are detected in the C IV profile. To keep the analysis simple, we do not try to get the column densities of individual components by fitting two components to the low dispersion data. Instead we estimate the total integrated column density in both the components.

For the absorption lines detected in the GHRS and FUSE data sets, we estimate column density at each velocity pixel using the relation

$$N(v) = 3.768 \times 10^{+14} \tau(v) / f\lambda \text{ cm}^{-2} \text{ km}^{-1} \text{ s} \quad (1)$$

where,  $\tau$ ,  $f$  and  $\lambda$  are the optical depth, oscillator strength and rest wavelength respectively. The latter two parameters have been taken from Verner et al. (1994). The total column density is obtained by integrating  $N(v)$  over the velocity range over which absorption is detected (see Table 2). The typical  $3\sigma$  errors are 25% of the estimates.

Although absorption is a direct indicator of the optical depth, in the case of partial coverage of the background source or when optical depth varies much more rapidly as a function of frequency than the spectral resolution, the depth of the absorption line provides only an under-estimate of the true column density. In case of poor spectral resolution, it is possible that the absorption in many cases may be actually optically thick. For example, for O VI  $\lambda\lambda 1031, 1037$  doublet detected in the GHRS data, the column density estimates for the members of the doublet just scale by their respective oscillator strengths. This suggests that the O VI absorption lines are actually saturated. Therefore, we take the estimated value based on O VI  $\lambda 1036$  as a lower limit.

Similar to O VI, it is possible that neutral hydrogen column density estimated from Ly $\beta$  and Ly $\gamma$  are at best the lower limits only. In the IUE spectrum, there is no apparent drop in the flux density at  $\sim 1250 \text{ \AA}$  corresponding to the Lyman edge absorption at the redshift of the quasar ( $z_{\text{em}} = 0.3700$ ) and the absorber ( $z_{\text{abs}} = 0.3654$ ). By taking  $20 \text{ \AA}$  on the blue side and  $50 \text{ \AA}$  on the red side of the expected Lyman edge, we find  $N(\text{H I}) \leq 3.06 \times 10^{16} \text{ cm}^{-2}$ . This is consistent with the  $N(\text{H I})$  values listed in Table 2 based on Ly $\beta$  and Ly $\gamma$ . Thus the actual value of  $N(\text{H I})$  is estimated to be between  $\sim 5 \times 10^{15} \text{ cm}^{-2}$  and  $3 \times 10^{16} \text{ cm}^{-2}$ .

We evaluate the upper limits for column densities of the species that are not detected using the Ly $\gamma$  absorption profile as the template (cf. Gupta et al. 2003). The scaling factor  $k = [Nf\lambda]_{X^i} / [Nf\lambda]_{\text{template}}$  between the two optical depths  $\tau_{\text{template}}$  and  $\tau_{X^i}$  for species  $X^i$  is then obtained by minimizing

$$\alpha = \Sigma(\tau_{X^i} - k * \tau_{\text{template}})^2 \quad (2)$$

The upper limits calculated in this manner are tabulated in Table 2.

**Table 2.** Column density estimates for the various species.

Species	N ( $\text{cm}^{-2}$ )	Instrument
Ly $\beta$	$2.57 \times 10^{15}$	HST-GHRS
Ly $\gamma$	$5.50 \times 10^{15}$	"
Lyman-Limit	$\leq 3.06 \times 10^{16}$	IUE
C IV	$\geq 1.14 \times 10^{15}$	HST-STIS
S VI	$8.62 \times 10^{13}$	HST-GHRS
O VI	$\geq 1.58 \times 10^{15}$	"
S IV	$\leq 9.32 \times 10^{13}$	"
P V	$\leq 2.91 \times 10^{13}$	"
N III	$\leq 1.30 \times 10^{14}$	"
N IV	$5.15 \times 10^{14}$	FUSE
Ne VIII	$5.45 \times 10^{15}$	"
S V	$\leq 4.01 \times 10^{13}$	"
O IV	$3.86 \times 10^{15}$	"

## 4.2 21 cm absorption

The column density of H I derived towards the optical point source is very low and the gas will not produce any detectable 21 cm absorption. A tentative detection of H I absorption (with a FWHM of  $100 \text{ km s}^{-1}$ ) towards 3C48 was reported by Pihlström (2001). High-resolution VLBI observations show that most of the radio emission is extended (Wilkinson et al. 1991; Worrall et al. 2004). Only 10% of the flux density at 1.53 GHz is in the collimated core-jet structure with only 1% of the flux density being associated with the radio core that is coincident with the optical point source. Thus the tentative detection of 21 cm absorption by Pihlström (2001), if true, has to be towards the extended radio emission.

Our deep GMRT observations fail to reveal any detectable 21 cm absorption at the systemic redshift of 3C48 as well as the gas responsible for UV absorption lines (Fig. 3). At the resolution of the GMRT observations, 3C48 is unresolved. Using the flux density of 20.3 Jy estimated from our observations, we obtain the  $3\sigma$  upper limit on optical depth to be in the range of 0.001 to 0.003. We obtain an upper limit on average  $N(\text{H I})$  across the radio source using

$$N(\text{H I}) = 1.82 \times 10^{18} T_s \tau_{\text{peak}} \Delta V \text{ cm}^{-2}. \quad (3)$$

Here  $\tau_{\text{peak}}$  is the peak optical depth,  $\Delta V$  the line FWHM in  $\text{km s}^{-1}$ ,  $T_s$  the spin temperature in K. Using the measured  $3\sigma$  upper limit on  $\tau$  (instead of  $\tau_{\text{peak}}$ ) we get  $N(\text{H I}) \lesssim 1.8 \times 10^{19} \text{ cm}^{-2}$  for  $\tau_{3\sigma} = 0.001$  and assuming  $T_s = 100 \text{ K}$  and  $\Delta V = 100 \text{ km s}^{-1}$ . This is consistent with low  $N(\text{H I})$  measured towards the optical point source. However, it should be noted that due to the extended nature of the radio source, low-resolution observations will fail to detect the presence of high  $N(\text{H I})$  gas in front of say knot B (at about 0.3 kpc from the compact core A: see Worrall et al. 2004), near which the jet gets disrupted. Knot B has a 1.53 GHz flux density of 250 mJy that is  $\sim 2\%$  of the total flux density. This then implies that  $\log N(\text{H I}) (\text{cm}^{-2}) < 21.30$  along our line of sight towards knot B. Thus our GMRT observations cannot rule out the presence of high column density H I towards individual knots or compact features.

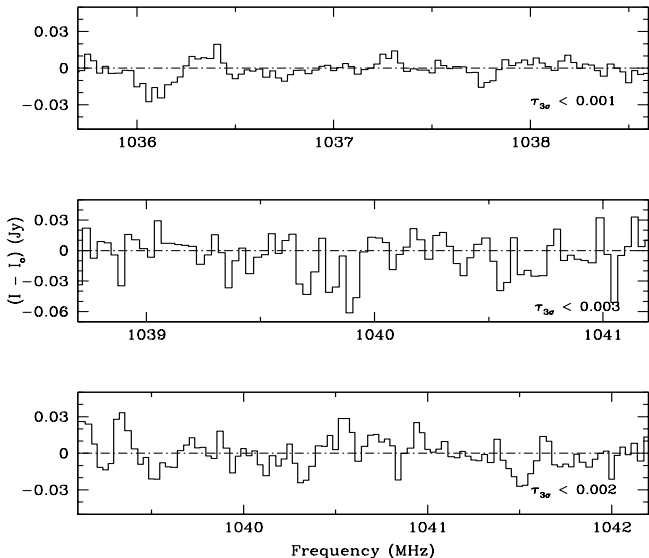


**Figure 3.** GMRT spectra covering the redshifted 21cm frequency corresponding to  $z_{em} = 0.3700$  from the optical emission lines,  $z_{em} = 0.3695$  from the CO emission spectrum (upper panel), and  $z_{abs} = 0.3654$  corresponding to the blue-shifted absorbing material reported here (middle and bottom panels).

## 5 DISCUSSION

The UV spectra show clear evidence of blue-shifted gas with  $z_{abs} = 0.3654$ . Compared with  $z_{em} = 0.3700$  this corresponds to a modest outflow velocity of  $\sim 1000 \text{ km s}^{-1}$ . We can further constrain the location of the outflowing material by comparing the absorption features with the emission lines. From Fig. 2, we can conclude that the members of the C IV  $\lambda\lambda 1548, 1550$  doublet have optical depths consistent with a full coverage of the background source. As C IV, Ly $\beta$  and O VI absorption lines are detected on top of the emission lines (see Fig. 4) complete coverage means that the gas is outside the broad-line region (BLR) and has a projected size more than that of the BLR (see Srianand & Shankaranarayanan 2000). We estimate the radius of BLR ( $R_{BLR}$ ) using the empirical relation

$$R_{BLR} = 27.4 \left( \frac{\lambda L_{5100}}{10^{44} \text{ ergs s}^{-1}} \right)^{0.68} \text{ lt days} \quad (4)$$

obtained by Corbett et al. (2003) using the reverberation mapping technique. The quasar rest frame luminosity at 5100 Å (i.e.  $L_{5100\text{Å}}$ ) is calculated using the observed flux density of  $F(8780 \text{ Å}) = 8.03 \times 10^{-16} \text{ ergs s}^{-1} \text{ Å}^{-1} \text{ cm}^{-2}$ , estimated from the STIS data set (05AB1030, program ID 8299; see Table 1) and a spectral index of 1.0. Substituting the numerical value of  $\lambda L_{5100\text{Å}} = 3.28 \times 10^{45} \text{ ergs s}^{-1}$  in equation (4), the radius of BLR is estimated to be 0.25 pc. Therefore we can conclude that size of the absorbing cloud should be larger than 0.5 pc and at least 0.25 pc away from the central engine.

In the following subsections we discuss the physical properties of the outflowing absorbing gas and explore the possibility that these might be affected by the interaction with the radio jet.

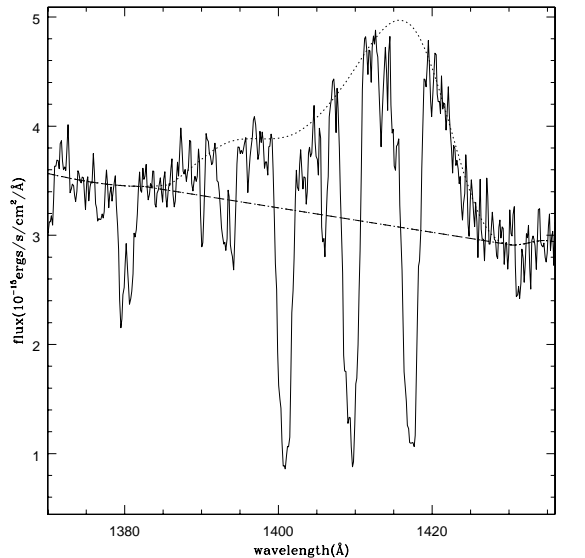


**Figure 4.** Portion of the HST GHRS spectrum showing Ly $\beta$  and O VI  $\lambda\lambda 1031, 1037$  absorption lines detected on top of the O VI emission line. The low-order polynomial used to fit the continuum to the spectrum and model the emission line is shown as the dotted line. Dashed line represents the fit to the underlying continuum emission.

### 5.1 Physical conditions of the absorber

The observed column densities of different species can be used to obtain physical conditions of the absorbing gas. As  $z_{abs} \approx z_{em}$  for the outflowing material, it is most likely that the ionization state of the gas will be influenced by the radiation field of the quasar. In addition, jet-cloud interaction can also play an important role in determining the observed kinematics and ionization state of the gas in radio sources. First we consider the case of the absorbing gas in photoionization equilibrium with the UV radiation from 3C48. For this purpose, we run grids of photoionization models using CLOUDY (Ferland 1996; Ferland et al. 1998) considering the gas to be ionised by a Mathews & Ferland (1987; hereinafter referred to as the MF) spectrum and having Solar abundances. The neutral hydrogen column density used is  $\log N(\text{H I}) = 16.0 \text{ cm}^{-2}$ . We present the results of our calculations in Fig. 5 as a function of the dimensionless quantity, the ionization parameter  $U$ , which is defined as

$$U = \frac{Q(H^{\circ})}{4\pi r^2 c n_{\text{H}}} \quad \text{where} \quad Q(H^{\circ}) = \int_{\nu_{LL}}^{\infty} \frac{L_{\nu}}{h\nu} d\nu \quad (5)$$

is the number of hydrogen ionizing photons per unit time,  $\nu_{LL}$  is the frequency corresponding to the Lyman edge and  $r$  is the distance from the central source. In the top panel of Fig. 5 we plot different column density ratios as a function of  $U$ . The vertical short dashed line in the right hand side of the figure marks the upper limit of  $U$  (i.e.  $\log U \leq -1.18$ ). Here we use the fact that  $N(\text{H I})/N(\text{H})$  cannot be less than  $10^{-4}$ . The constraint on the total hydrogen column density,  $N(\text{H})$ , comes from the Chandra observations of Worrall et al. (2004). They find no evidence for any intrinsic absorption in excess of  $5 \times 10^{19} \text{ cm}^{-2}$  in the direction of 3C48. A conservative lower limit of  $\log U = -1.82$  is ob-

tained from the column density ratios  $N(\text{N IV})/N(\text{N III})$  and  $N(\text{S VI})/N(\text{S IV})$ . From Fig. 5, it is apparent that the ratio  $N(\text{C IV})/N(\text{N IV})$  is independent of  $U$  when  $\log U \leq -1.0$ . As the gas is optically thin our choice of  $N(\text{H I})$  and Solar abundance ratios,  $Z_{\odot}$  will not alter these constraints. The observed ratio of  $N(\text{C IV})/N(\text{N IV})$  is  $\sim 0.1$  dex below the predictions of our model. This is within the measurement uncertainties of our data. Therefore, within the measurement uncertainties,  $[\text{N}/\text{C}]$  is very close to Solar values. This is in contrast with the systematically higher supersolar  $[\text{N}/\text{C}]$  ratios observed in most of the QSOs, especially the ones at high redshift or having high luminosities (Hamann & Ferland 1992, 1993, 1999; Petitjean & Srianand 1999). The rapid star-formation models enhancing the nitrogen abundance by the secondary CNO nucleosynthesis have been used to explain the  $[\text{N}/\text{C}] > [\text{N}/\text{C}]_{\odot}$  ratios in these high redshift/luminosity systems. Using the observed flux density,  $F(1246.7\text{\AA}) = 3.13 \times 10^{-15} \text{ erg s}^{-1} \text{ cm}^{-2} \text{ \AA}^{-1}$  from the IUE data, a luminosity distance of 1950.7 Mpc and a spectral index of  $\alpha = 0.5$ , we estimate the luminosity,  $\nu L_{\nu}$ , at 1450  $\text{\AA}$  for 3C48 to be  $3.5 \times 10^{11} L_{\odot}$ . From Fig. 7 of Hamann et al. (1999), it can be seen that Solar values of  $[\text{N}/\text{C}]$  are not unusual for 3C48 with  $z_{\text{em}} = 0.3700$  and above estimated luminosity at 1450  $\text{\AA}$ . In the bottom panel of Fig. 5, we plot the predicted values of column densities of various species as a function of  $U$ . Horizontal lines mark the observed values. Clearly, observed column densities of C IV and S VI are lower by  $\sim 0.5$  dex compared to the model predictions within the allowed range of ionization parameter. As the absorbing gas is optically thin, this difference can be accounted for by lowering either the value of  $N(\text{H I})$  or the metallicity. The allowed range of  $N(\text{H I})$  listed in Table 2, constrains the metallicity of the absorbing gas to be in range  $0.1 \leq Z/Z_{\odot} \leq 1.3$ .

The column density of Ne VIII as predicted by the photoionization models is more than two orders of magnitude lower than the Ne VIII column density estimated from the possible detection of this line. Reconciliation of the observed Ne VIII value requires neon abundance enhancement or optically ionized regions with different levels of ionisation (multiply-ionized regions). Since the rest of the observed species can be explained by Solar abundance ratios it seems unlikely that only Ne has an unusual abundance. Thus the possible detection of Ne VIII in the poor signal-to-noise ratio FUSE data can be understood by the existence of multiply-ionized regions. Such multiply-ionized regions have been used to explain the observed column densities of highly ionised species (including Ne VIII) in J2233–606, UM675 and 3C288.1 (Petitjean & Srianand 1999; Hamann et al. 1997; Hamann et al. 2000). Thus it is possible that the low-ionization species originate from the high-density (low-ionization) phase and high-ionization species Ne VIII originate from the low-density (high-ionization) phase of the absorption-line system. Our data does show some evidence that the absorption-line system consists of a number of components. However, due to low spectral resolution and poor signal-to-noise ratio it is difficult to say if Ne VIII arises from the same component as the other low-ionization species. The density of the absorbing gas or its distance from the quasar nucleus can, in principle, be constrained using equation (5) if either of these two quantities and  $Q(\text{H}^{\circ})$  are known. We estimate the luminosity at the Lyman limit,  $L_{\text{LL}} = 5.4 \times 10^{29} \text{ erg s}^{-1} \text{ Hz}^{-1}$  in the quasar rest frame using the observed flux density,

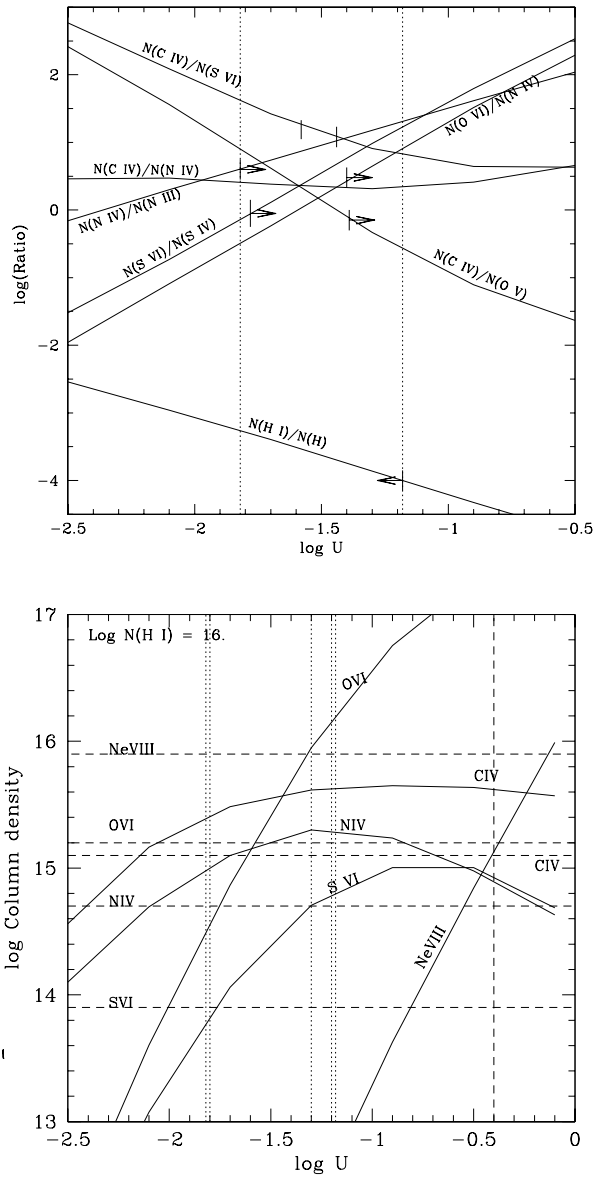


**Figure 5.** Results of model calculations with  $N(\text{H I}) = 10^{16} \text{ cm}^{-2}$ , QSO spectrum given by MF and  $Z = Z_{\odot}$ . Top panel shows different ion ratios predicted in the calculations as a function of ionization parameter. The arrows indicate the limits on  $U$  from the observed values. The vertical dashed lines mark the possible range in  $U$  that will be consistent with the observations. Lower panel shows the predicted column density as a function of  $U$  for a few ions. The horizontal lines mark the measured values or upper limits to the column densities (see Table. 2). Apart from  $N(\text{Ne VIII})$  all the observed column densities and the limits are consistent with  $-1.82 \leq \log U \leq -1.18$  and  $Z = 0.5 Z_{\odot}$  for  $\log N(\text{H I}) = 16 \text{ cm}^{-2}$ .

$F(1246.7\text{\AA}) = 3.13 \times 10^{-15} \text{ erg s}^{-1} \text{ cm}^{-2} \text{ \AA}^{-1}$  from the IUE data, a luminosity distance of 1950.7 Mpc and a spectral index of  $\alpha = 0.5$ . This translates into  $Q(\text{H}^{\circ}) = 1.3 \times 10^{56} \text{ photons s}^{-1}$ . Substituting numerical values in equation (5) then gives

$$U = \frac{3.4 \times 10^{44}}{nr^2}. \quad (6)$$

Taking a nominal value of  $\log U = -1.5$  from the photoionization models,  $n_{pc}^2 = 1.2 \times 10^9 \text{ cm}^{-3} \text{ pc}^2$ , where  $r_{pc}$  is the distance from the central source in parsecs. However, with the available information, it is not possible to get useful estimates of these parameters. Assuming that the absorbing cloud was pushed outwards by the radio jet  $\gtrsim 10^5$  yr ago (cf. Section 5.2), it would have travelled  $\gtrsim 100$  pc with a velocity of  $\sim 1000 \text{ km s}^{-1}$ . This implies that the number density  $n \lesssim 10^5 \text{ cm}^{-3}$ .

## 5.2 Jet-cloud interaction?

The complex radio structure of 3C48 has led to suggestions that the jet in 3C48 may be disrupted by strong interaction with the external medium (e.g. Wilkinson et al. 1991; Feng et al. 2005). This is not surprising as CSSs tend to be more asymmetric in both the separation ratio ( $r_D$ ), defined to be the ratio of the separation from the core/nucleus of the farther component to the nearer one, and the flux density ratio ( $r_L$ ), defined to be the ratio of integrated flux densities of the farther to the nearer component, compared with the larger sources, suggesting interaction with an asymmetric distribution of gas in the central regions (Saikia et al. 1995, 2001). The component nearer to the nucleus often tends to be the brighter one, which is possibly a signature of the expansion of nearer component through the denser environment leading to higher dissipation of energy. Orientation effects can also lead to substantial enhancements in these observed asymmetry parameters (cf. Jeyakumar et al. 2005 and references therein). Using the images and core position as given by Feng et al. (2005), who have recently reported the detection of a counter-jet in 3C48, the separation ratio for the prominent northern peak N2 and the counter-jet S is  $\approx 2.8$ . This could increase to  $\approx 5$  if the region of enhanced intensity in the outer region is taken instead of N2. The flux density ratio ( $r_L$ ) of the northern or approaching components to the southern one, S, lies between  $\sim 200$  and  $400$  for observations at different frequencies and with different resolutions (Feng et al. 2005). The source also appears significantly misaligned, possibly due to collision with clouds of gas and also exhibits jitters in the direction of the ejection axis as seen in the VLBA 8-GHz image of Worrall et al. (2004). The misalignment angle, defined to be the supplement of the angle formed at the core by N2 and S is about  $30^\circ$ . For an inclination angle of  $30-35^\circ$  for the jet, estimated from the relative strength of the core, and an intrinsic misalignment of  $\sim 10-15^\circ$ ,  $r_D$  is in the range of  $\sim 3.8$  to  $5$  for a velocity of advancement of  $\sim 0.5c$ . The corresponding flux density ratio,  $r_L = r_D^{2+\alpha}$  (e.g. Scheuer & Readhead 1979; Blandford & Königl 1979) is in the range of  $\sim 50-100$  for a spectral index of  $0.9$ , which is lower than the observed flux density ratio by at least a factor of  $\sim 3$ . This difference could be attributed to intrinsic asymmetries in the gas distribution (cf. McCarthy, van Breugel & Kapahi 1991). Using the formalism of Eilek & Shore (1989) and Gopal-Krishna & Wiita (1991), we estimate the density ratio on opposite sides to be  $\sim 7$ . However, these numbers should be treated with caution because of the complex structure of the source and uncertainties in some of the basic parameters such as the velocity of advancement.

The detection of blue-shifted absorption lines caused by clouds of gas in the path of the radio jet would be

an indication of jet-cloud interaction. Chatzichristou et al. (1999) report the detection of blue-shifted emission line ([OIII]  $\lambda\lambda 4959, 5007$  and [OII]  $\lambda 3727$ ) gas in 3C48 over  $1.9 \text{ arcsec}^2$  of the central region. On the basis of the velocity structure of the blue-shifted component of the emission line gas and its increasing strength in the same direction as the radio jet, they suggest that this gas contains the imprint of interaction with the jet. The kinematical properties of this blue-shifted emission line gas, which shows clumpy morphology and has an outflow velocity of  $\sim 580 \text{ km s}^{-1}$ , are similar to the one detected in absorption. Using the mass estimate of  $\sim 10^9 M_\odot$  (Fabian et al. 1987) for the emission line gas, determined from the strength of [OIII]  $\lambda 5007$  in 3C48, Wilkinson et al. (1991) show that energetics of the radio jet are capable of driving this gas with velocities as high as  $\approx 1000 \text{ km s}^{-1}$ . This is similar to the outflowing velocity of  $\sim 1000 \text{ km s}^{-1}$  for the blue-shifted material seen in absorption. Although blue-shifted absorption can be caused by other physical processes like radiative acceleration, the kinematical similarities with the emission-line gas and the situation in 3C48 make jet-cloud interaction a likely possibility.

The interaction with the jet can impart momentum to the gas and can also heat as well as ionize it. The gas ploughed and compressed by the jet can heat up to post-shock temperatures of  $\sim 10^8 \text{ K}$  (de Vries et al. 1999). Taking adiabatic and radiative cooling into account de Vries et al. find that such a gas with a density of  $1-5 \text{ cm}^{-3}$  will cool to  $10^4 \text{ K}$  in about  $30,000$  yr. Using the recombination coefficients from Péquignot, Petitjean & Boisson (1991), we find that the recombination timescales for gas with a temperature few times  $10^4 \text{ K}$  and density  $5 \text{ cm}^{-3}$  are only a few thousand years for most of the species considered here. The maximum recombination timescale occurs for H I and O I, which we estimate to be  $\sim 10^4$  yr. Therefore, any thermal or ionization signature of jet-cloud interaction will be lost in timescales  $\gtrsim 10^5$  yr. Since we can explain the observed column densities of the absorbing cloud using the photoionization models alone, any injection of energy resulting from a jet-cloud interaction must have taken place before  $10^5$  yr.

## 6 SUMMARY

We have reported the detection of a  $z_{\text{abs}} = 0.3654$  absorption-line system in the UV spectrum of the CSS quasar 3C48, which has a highly distorted radio structure. The absorbing material is blueshifted by  $\sim 1000 \text{ km s}^{-1}$  with respect to  $z_{\text{em}} = 0.3700$  estimated from the optical emission lines. The outflowing material shows absorption lines from Ly $\beta$ , Ly $\gamma$ , C IV, S VI, O VI, N IV and possibly O IV and Ne VIII. Detection of high-ionization lines such as O VI and Ne VIII suggests that the outflowing material is located close to the nucleus of the quasar. The kinematical properties of the  $z_{\text{abs}} = 0.3654$  system are very similar to the blue-shifted emission line gas detected by Chatzichristou et al. (1999). The complex radio structure has been interpreted to be due to strong interaction with the ambient medium. On the basis of spatial correlation between the radio source and emission line gas, Chatzichristou et al. argue that this component bears the imprint of the interaction between the jet and the ambient gas. Considering the similarity of the kinematics of the



emitting and absorbing material and the physical situation in 3C48, it is possible that the outflowing material detected in absorption may have also interacted with the radio jet.

Interaction of a cloud with a radio jet can impart momentum and as well as heat and ionize it. The recombination and cooling timescales suggest that signatures of such a jet-cloud interaction will be lost on time scales  $\gtrsim 10^5$  yr. We find that photoionization models with Solar abundance ratios (with overall metallicity in the range  $0.1 \leq Z/Z_{\odot} \leq 1.3$ ) are enough to explain the observed column densities of all the species except for Ne VIII. The consistency with the photoionization-models suggests that the any possible interaction of absorbing material with the jet must have taken place  $\gtrsim 10^5$  yr ago. Reconciliation of the possible Ne VIII detection requires regions with different levels of ionization. We also find that the abundance ratio of nitrogen to carbon is close to Solar values, unlike in the case of most quasars, especially at high-redshifts, which have super-Solar values.

Our GMRT spectra of 3C48, from which we estimate the  $3\sigma$  upper limit to the optical depth to lie in the range 0.001 to 0.003, is consistent with the low N(H I) detected towards the optical point source. Assuming a spin temperature of 100 K and line width of  $100 \text{ km s}^{-1}$ , these correspond to column densities of  $N(\text{H I}) \leq (1.8-5.4) \times 10^{19} \text{ cm}^{-2}$ . Due to the diffuse nature of the radio structure of 3C48, H I column densities as high as  $10^{21} \text{ cm}^{-2}$  towards individual knots or compact features cannot be ruled out.

## ACKNOWLEDGMENTS

We thank an anonymous referee for several useful comments and suggestions. We are grateful to MAST archive for the excellent user support and documentation. We also thank the numerous contributors to GNU/Linux group. This research has made use of the NASA/IPAC Extragalactic Database (NED) which is operated by the Jet Propulsion Laboratory, California Institute of Technology, under contract with the National Aeronautics and Space Administration. One of us (NG) thanks the Kanwal Reiki Scholarship of TIFR for partial financial support. We also thank the GMRT staff for their cooperation during our GMRT observations. The GMRT is a national facility operated by the National Centre for Radio Astrophysics of the Tata Institute of Fundamental Research.

## REFERENCES

- Arshakian T.G., Longair M.S., 2000, MNRAS, 311, 846  
 Axon D.J., Capetti A., Fanti R., Morganti R., Robinson A., Spencer R., 2000, AJ, 120, 2284  
 Baker J.C., Hunstead R.W., Athreya R.M., Barthel P.D., de Silva E., Lehnert M.D., Saunders R.D.E., 2002, ApJ, 568, 592  
 Blandford R.D., Königl A., 1979, ApJ, 232, 34  
 Boroson T.A., Oke J.B., 1982, Nature, 296, 397  
 Briggs D.S., 1995, AAS, 18711202B  
 Carvalho J.C., 1998, A&A, 329, 845  
 Chatzichristou E.T., Vanderriest C., Jaffe W., 1999, A&A, 343, 407  
 Conway J.E., Myers S.T., Pearson T.J., Readhead A.C.S., Unwin S.C., Xu W., 1994, ApJ, 425, 568  
 Corbett E.A. et al., 2003, MNRAS, 343, 705  
 Cotton W.D., Spencer R.E., Saikia D.J., Garrington S., 2003, A&A, 403, 537  
 Dallacasa D., Fanti C., Fanti R., Schilizzi R.T., Spencer R.E., 1995, A&A, 295, 27  
 de Vries W.H., O’Dea C.P., Baum S.A., Barthel P.D., 1999, ApJ, 526, 27  
 Eilek J.A., Shore S.N., 1989, ApJ, 342, 187  
 Fabian A.C., Crawford C.S., Johnstone R.M., Thomas P.A., 1987, MNRAS, 228, 963  
 Fanti R., Fanti C., Schilizzi R.T., Spencer R.E., Nan Rendong, Parma P., van Breugel W.J.M., Venturi T., 1990, A&A, 231, 333  
 Fanti C., Fanti R., Dallacasa D., Schilizzi R.T., Spencer R.E., Stanghellini C. 1995, A&A, 302, 317  
 Fanti C. et al., 2004, A&A, 427, 465  
 Feng W.X., An T., Hong X.Y., Zhao Jun-Hui, Venturi T., Shen Z.Q., Wang W.H., 2005, A&A, 434, 101  
 Ferland G.J., 1996, HAZY- a brief introduction to CLOUDY 90, University of Kentucky Physics Department Internal Report  
 Ferland G.J., Korista K.T., Verner D.A., Ferguson J.W., Kingdon J.B., Verner E.M., 1998, PASP, 110, 761  
 Gelderman R., Whittle M., 1994, ApJS, 91, 491  
 Gopal-Krishna, Wiita P.J., 1991, ApJ, 373, 325  
 Greenstein J.L., Mathews T.A., 1963, Nature, 197, 1041  
 Gupta N., Srianand R., Petitjean P., Ledoux C., 2003, A&A, 406, 65  
 Hamann F., Ferland G.J., 1992, ApJ, 391, 53  
 Hamann F., Ferland G.J., 1993, ApJ, 418, 11  
 Hamann F., Ferland G.J., 1999, ARA&A, 37, 487  
 Hamann F., Barlow T.A., Junkkarinen V., Burbidge E.M., 1997, ApJ, 478, 80  
 Hamann F.W., Netzer H., Shields J. C., 2000, ApJ, 536, 101  
 Higgins S.W., O’Brien T.J., Dunlop J.S., 1999, MNRAS, 309, 273  
 Jeyakumar S., Wiita P.J., Saikia D. J., Hooda J.S., 2005, A&A, 432, 823  
 Junor W., Salter C.J., Saikia D. J., Mantovani F., Peck A. B., 1999, MNRAS, 308, 955  
 Mantovani F., Junor W., Fanti R., Padrielli L., Saikia D.J., 1994, A&A, 292, 59  
 Mathews W.G., Ferland G.J., ApJ, 1987, 323, 456  
 Mathews T.A., Sandage A.R., ApJ, 1963, 138, 30  
 McCarthy P.J., van Breugel W., Kapahi V.K., 1991, ApJ, 371, 478  
 Neugebauer G., Soifer B.T., Miley G. K., 1985, ApJ, 295, L27  
 O’Dea C.P. 1998, PASP, 110, 493  
 O’Dea C.P. et al., 2002, AJ, 123, 2333  
 Orienti M., Dallacasa D., Fanti C., Fanti R., Tinti S., Stanghellini C., 2004, A&A, 426, 463  
 Péquignot D., Petitjean P., Boisson C., 1991, A&A, 251, 680  
 Petitjean P., Riediger R., Rauch, M., 1996, A&A ,307, 417  
 Petitjean P., Srianand R., 1999, A&A, 345, 73  
 Phillips R.B., Mutel R.L., 1982, A&A, 106, 21  
 Pihlström, Y.M., 2001, PhD Thesis, Chalmers University of Technology

- Readhead A.C.S., Taylor G.B., Xu W., Pearson T.J., Wilkinson P.N., Polatidis A.G., 1996a, *ApJ*, 460, 612
- Readhead A.C.S., Taylor G.B., Pearson T.J., Wilkinson P.N., 1996b, *ApJ*, 460, 634
- Saikia D.J., Jeyakumar S., Wiita P.J., Sanghera H.S., Spencer R.E., 1995, *MNRAS*, 276, 1215
- Saikia D.J., Jeyakumar S., Salter C.J., Thomasson P., Spencer R.E., Mantovani F., 2001, *MNRAS*, 321, 37
- Saikia D.J., Gupta N., 2003, *A&A*, 405, 499
- Sanghera H.S., Saikia D.J., Lüdke E., Spencer R.E., Foulsham P.A., Akujor C.E., Tzioumis A.K., 1995, *A&A*, 295, 629
- Scheuer P.A.G., Readhead A.C.S., 1979, *Nature*, 277, 182
- Scoville N.Z., Padin S., Sanders D.B., Soifer B.T., Yun M.S., 1993, *ApJ*, 415, L75
- Snellen I.A.G., Schilizzi R.T., van Langevelde H.J., 2000a, *MNRAS*, 319, 429
- Snellen I.A.G., Schilizzi R.T., Miley G.K., de Bruyn A.G., Bremer M.N., Röttgering H.J.A., 2000b, *MNRAS*, 319, 445
- Spencer R.E., McDowell J.C., Charlesworth M., Fanti C., Parma P., Peacock J.A., 1989, *MNRAS*, 240, 657
- Spergel et al., 2003, *ApJS*, 148, 175
- Srianand R., Shankaranarayanan S., 1999, *ApJ*, 518, 672
- Stanghellini C., Dallacasa D., O’Dea C.P., Baum S.A., Fanti R., Fanti C., 2001, *A&A*, 379, 870
- Stockton A., Ridgway S.E., 1991, *AJ*, 102, 488
- Taylor G.B., Readhead A.C.S., Pearson T.J., 1996, *ApJ*, 463, 95
- Telfer R.C., Kriss G.A., Zheng W., Davidsen A.F., Green R.F., 1998, *ApJ*, 509, 132
- Thuan T.X., Oke J.B., Bergeron J., 1979, 230, 340
- Tytler D., Boksenberg A., Sargent W.L.W., Young P., Kunth D., 1987, *ApJS*, 64, 667
- van Ojik R., Roettgering H.J.A., Miley G.K., Hunstead R.W., 1997, *A&A*, 317, 358
- Verner D.A., Barthel P.D., Tytler D., 1994, *A&AS*, 108, 287
- Wampler E.J., Robinson L.B., Burbidge E.M., Baldwin J.A., 1975, *ApJL*, 198, L49
- Wang Z., Wiita P.J., Hooda J.S., 2000, *ApJ*, 534, 201
- Wilkinson P.N., Tzioumis A.K., Benson J.M., Walker R.C., Simon R.S., Kahn F.D., 1991, *Nature*, 352, 313
- Wilkinson P.N., Polatidis A.G., Readhead A.C.S., Xu W., Pearson T.J., 1994, *ApJ*, 432, L87
- Wink J.E., Guilloteau S., Wilson T.L., 1997, *A&A*, 322, 427
- Worrall D.M., Hardcastle M.J., Pearson T.J., Readhead A.C.S., 2004, *MNRAS*, 347, 632